Chinese Chemical Letters 32 (2021) 999–1009

Contents lists available at ScienceDirect

Chinese Chemical Letters

journal homepage: www.elsevier.com/locate/cclet

Review

Bifunctional air electrodes for flexible rechargeable Zn-air batteries

Xiaoling Lang[a], Zhibiao Hu[a], Caiyun Wang[b,*]

[a] Fujian Provincial Key Laboratory of Clean Energy Materials, Longyan University, Longyan 364000, China
[b] ARC Centre of Excellence for Electromaterials Science, Intelligent Polymer Research Institute, AIIM Facility, Innovation Campus, University of Wollongong, North Wollongong, NSW 2500, Australia

ARTICLE INFO

Article history:
Received 28 July 2020
Received in revised form 28 September 2020
Accepted 9 October 2020
Available online 10 October 2020

Keywords:
Zn-air batteries
Flexible air electrodes
Bifunctional catalysts
Carbon materials
Metal oxides

ABSTRACT

Flexible rechargeable Zn-air batteries are considered as one of the most promising battery systems to drive flexible and wearable electronic devices owing to their high safety, high gravimetric energy density, low self-discharge and low cost. One of the key challenges is to develop air electrodes with high performance and high mechanical flexibility. This minireview discusses the recent progress in the design and fabrication of flexible air electrodes. It focuses on the latest innovations in bifunctional oxygen reduction reaction and oxygen evolution reaction electrocatalysts, mainly including carbon-based materials (*e.g.*, heteroatom-doped carbon, metal-nitrogen moieties doped carbon), metal oxides (*e.g.*, spinel oxides, perovskite oxides) and their composites. It aims to provide an insight into the structure-property relationship of bifunctional catalysts. We also discuss the challenges and future perspectives.

1. Introduction

Currently there has been an ever-growing market for flexible and wearable electronics such as roll-up displays, e-textiles, wearable sensors and human interaction devices [1–9]. These flexible devices can be rolled, bent or twisted while maintaining their functions, which are accelerating revolutionary changes in our life. A reliable and stable power supply is an indispensable part of these devices. Amongst various power sources, flexible metal-air batteries are considered as one of the most promising candidates due to high gravimetric energy density and light weight [10–18]. In particular, flexible zinc-air (Zn-air) batteries are highly attractive, as they are safer compared to lithium-air and sodium-air batteries that involve the use of flammable electrolytes [17,19–24]. They can be charged more efficiently in an alkaline electrolyte compared to magnesium-air and aluminum-air batteries [25–27]. Zn-air battery has a theoretical energy density of 1218 Wh/kg, three times higher than that of the widely used Li ion battery (400 Wh/kg) but at a much lower manufacturing cost of 160–200 US$ kW/h in contrast to that 400–800 US$ kW/h for Li ion battery [15,25]. Therefore, Zn-air batteries are considered as a next generation battery technology beyond lithium batteries, and flexible Zn-air batteries is a promising energy storage system to drive the above mentioned flexible and wearable electronics (Fig. 1).

A Zn-air battery involves the dissolution and deposition of Zn at anode, oxygen reduction reaction (ORR) and oxygen evolution reaction (OER) at air cathode in an alkaline electrolyte (Fig. 1). During the discharge process, oxidation of Zn occurs at anode (Eqs. 1 and 2), and the released electrons travel through an external circuit to air electrode. The generated hydroxide ions migrate to Zn electrode, forming zincate ions ($Zn(OH)_4^{2-}$) (Eq. 1), which further decompose into insoluble zinc oxide (ZnO) (Eq. 2). Meanwhile, oxygen molecules diffuse to air electrode and are reduced to form hydroxide ions (Eq. 3) at the three-phase boundary between oxygen (gas), electrolyte (liquid), and active material (solid). An equilibrium potential of 1.65 V is generated from the overall reaction (Eq. 4). Reverse reactions (Eqs. 5–7) are involved in the charge process for Zn-air batteries [25].

During the discharge process:

At Zn-electrode

$$Zn + 4OH^- \rightarrow Zn(OH)_4^{2-} + 2e^- \quad (1)$$

$$Zn(OH)_4^{2-} \rightarrow ZnO + H_2O + 2OH^- \quad (2)$$

At air-electrode

$$O_2 + 2H_2O + 4e^- \rightarrow 4OH^- \quad (3)$$

$$\text{Overall reaction: } 2Zn + O_2 \rightarrow 2ZnO \ (E = 1.65\,V) \quad (4)$$

During the charge process:

* Corresponding author.
E-mail address: caiyun@uow.edu.au (C. Wang).

https://doi.org/10.1016/j.cclet.2020.10.005
1001-8417/

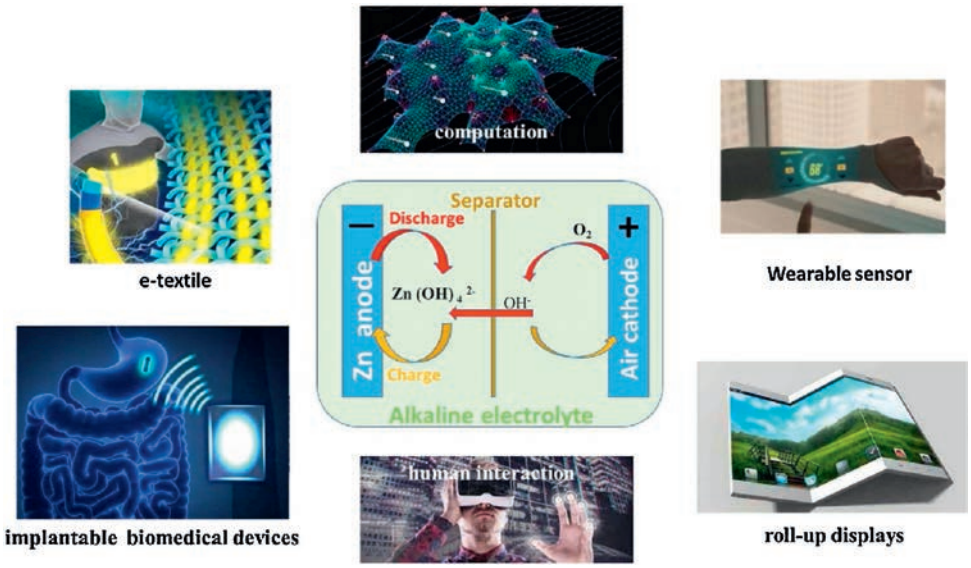

Fig. 1. Schematic illustration of the working principle of Zn-air batteries and their potential applications.

At Zn-electrode

$$ZnO + H_2O + 2e^- \rightarrow Zn + 2OH^- \quad (5)$$

At air-electrode

$$4OH^- \rightarrow O_2 + 2H_2O + 4e^- \quad (6)$$

Overall reaction:

$$2ZnO \rightarrow 2Zn + O_2 \quad (7)$$

Currently air electrodes for Zn-air batteries face challenges of large over-potentials, low energy efficiencies and low cycle stabilities, owing to the sluggish kinetics of ORR and OER that are determined by properties of electrocatalysts. Hence electrocatalysts with both high catalytic ability to ORR and OER have being extensively explored for decades [28–37]. The electrochemical reduction and evolution of oxygen under alkaline conditions are very complicated that involves two reaction pathways: a four-electron reaction (Eq. 8) and a two-electron reaction (Eqs. 9–11). Oxygen is directly reduced to OH^- *via* a $4e^-$ transfer with an equilibrium potential of 0.401 V *versus* reversible hydrogen electrode (RHE). However, the two-electron reaction pathway involves two steps and produces OH^- or HO_2^-, which reduces the ORR and OER efficiency. Moreover, the membrane separator used in the battery system can be destroyed due to the strong oxidizing agent of HO_2^-, thus leading to limited cycle life [38,39]. Therefore, the four-electron reduction pathway is highly preferred for realizing high efficiency as well as avoiding the premature degradation of batteries [40].

Four-electron reduction pathway :

$$O_2 + 2H_2O + 4e^- \rightarrow 4OH^- \; E^0 = 0.401\ V \quad (8)$$

Two-electron reduction pathway :

$$O_2 + H_2O + 2e^- \rightarrow HO_2^- + OH^- \; E^0 = 0.076\ V \quad (9)$$

$$HO_2^- + H_2O + 2e^- \rightarrow 3OH^- \; E^0 = 0.878\ V \quad (10)$$

$$2HO_2^- \rightarrow 2OH^- + O_2 \quad (11)$$

The sluggish ORR and OER reactions of air electrodes can be ascribed to the strong O=O bond (498 kJ/mol) [15,41,42]. For flexible/wearable batteries application, these air electrodes should be with a high level of flexibility in addition to the high electrochemical performance.

There have been quite a few excellent review articles regarding to the configuration and performance of Zn-air batteries [24,43,44] and flexible metal-air batteries [27,45–48]. These reviews mainly focused on the design of flexible metal-air battery components, such as electrodes (carbon-based and non-carbon-based electrodes) [27,46], electrolytes (liquid and solid-state electrolytes) [46] and configurations (planar, woven-type, cable-type and sandwich structure) [24,45,46]. So far, few dedicated reviews about the bifunctional electrocatalyst-based flexible air electrodes for flexible Zn-air battery are available. Therefore, it is the time to summarize the recent progress in such air electrodes for flexible and wearable Zn-air batteries. This review focuses on two widely investigated catalysts including carbon based and metal oxide-based materials.

2. Carbon-based materials

Carbon nanomaterials have been widely explored as electrocatalysts for ORR owing to their good electrocatalytic ability, abundance, low cost and environmental friendliness [49]. Their use as oxygen electrocatalysts for wearable Zn-air batteries have attracted attention due to their intrinsically flexible nature and catalytic ability [48,50]. However, carbon materials catalyze the ORR reaction mostly through a two-electron pathway and generate H_2O_2, and thus offer poor OER catalytic activity [39,51]. They also suffer from the carbon corrosion problem under the oxidation potentials of OER, which can cause the catalysts agglomeration blocking active sites thus deactivating the catalytic ability [52,53]. Therefore, different approaches have been applied to improve their electrocatalytic properties mainly from two aspects: regulating electronic structure of carbon atoms and increasing the number of active sites. This material family mainly include heteroatom-doped carbons and metal-nitrogen moieties doped carbon materials [28–30,54–59].

2.1. Heteroatom-doped carbons

The doping of heteroatoms into carbon materials is a widely used strategy to achieve high electrocatalytic activity for ORR and OER by regulating the electronic structure of carbon atoms [55,60–65]. The commonly incorporated heteroatoms mainly include N, P, S and B [15,22,29,57,66–68]. The regulated carbon atoms are believed to be the active sites responsible for the excellent electrocatalytic activity. These heteroatoms can create net positive charge around carbon atoms leading to improved chemisorption of oxygen and electron transfer [65,68]. More importantly, the heteroatom-doping can greatly boost the ORR activity leading to favorable formation of OH^- *via* the four-electron pathway, especially for N-doped carbon materials [63,69]. In addition to single atom doping, the doping of binary (*e.g.*, P/N, B/N and S/N) and ternary (*e.g.*, P/B/N, B/F/N) heteroatoms into carbon materials have also been verified as an efficient strategy to achieve outstanding electrocatalytic activity and stability for Zn-air batteries [31,62,63,70–75], owing to the synergistic electronic interactions between different dopants and adjacent carbon atoms [76]. Herein, we will focus on discussing the electrocatalytic performance as well as the flexibility and mechanical strength of air electrodes with heteroatom-doped carbon material catalysts.

Liu *et al.* [50] developed a flexible nanoporous carbon nanofiber film (denoted as NCNF) with a large specific surface area of 1249 m^2/g by high temperature pyrolysis of the electrospun polyimide fiber films. These films were highly flexible and mechanically strong (Figs. 2a and b). They could recover the original state even after being repeatedly bent for more than 500 times. Such high flexibility may be related to the polar interactions associated with the constituents of oxygen, nitrogen, and/or hydrogen atoms along the polymer backbone. This material displayed an excellent ORR performance *via* a four-electron efficient pathway with an onset potential of 0.97 V and a high current density of 4.7 mA/cm^2, as well as an excellent OER performance with an onset voltage of 1.43 V at 10 mA/cm^2, which were better than commercial Pt/C (ORR current density of 4.4 mA/cm^2) and IrO_2 (OER onset voltage of 1.50 V at 10 mA/cm^2). It is worth mentioning that the assembled all-solid-state Zn-air battery with NCNF film air cathode, Zn foil anode and alkaline poly (vinyl alcohol) (PVA) gel electrolyte, exhibited stable charge and discharge potentials for 6 h even when the battery was being bent or folded back and forth (Fig. 2c). After 500 cycles (about 83 h), the NCNF air-cathode showed a slight performance loss with a small increase in the voltage gap by 0.13 V. These results demonstrate that NCNF-based Zn-air batteries have the potential for application in flexible and wearable electronic equipment.

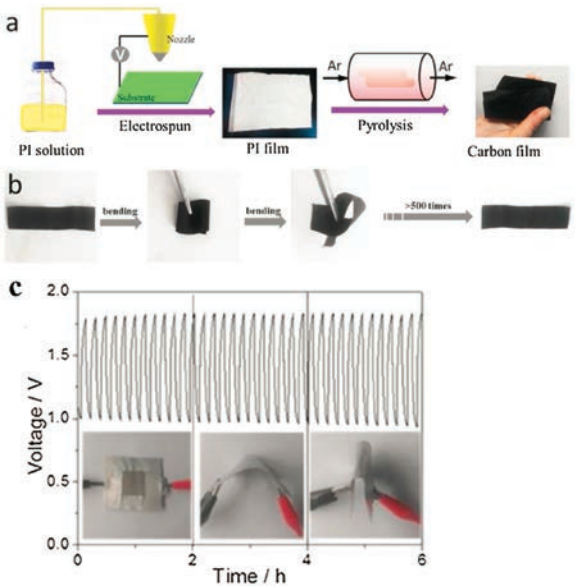

Fig. 2. (a) Schematic illustration of the fabrication procedure toward the NCNF. (b) Photographs of flexible NCNF film. (c) Galvanostatic discharge-charge curves for Zn-air battery with NCNF-1000 as catalyst under different bending strain. Adapted with permission [50]. Copyright 2016, John Wiley and Sons.

The mechanism of nitrogen heteroatoms for promoting the electrocatalytic activity of carbon to ORR and OER have been investigated and elucidated by many researchers [68,77–79]. It is generally believed that the doping of nitrogen into carbon creates a positive charge nearby carbon atoms, which favors the chemisorption of oxygen and electron transfer [80]. During the charge process, it can easily adsorb OH^- onto N-doped carbon materials surface, as well as facilitate the transfer of intermediates such O_2^{2-} and O^{2-} [81]. Therefore, the modulated carbon atoms by nitrogen atoms provide more active sites with enhanced charge transfer, leading to improved electrocatalytic activity for ORR and OER.

Combining N with another heteroatom, like P or S, forming co-doped carbon can further change the surface electronic states and polarities of carbon atoms for improved electrochemical performance. Chen *et al.* reported nitrogen and phosphorous co-doped carbon spheres (NPCS) which exhibited better electrocatalytic performance than that of commercial Pt/C and RuO_2 [28]. They first prepared porous polyaniline particles in the presence of phytic acid, and then N, P co-doped carbon spheres by pyrolysis. Theoretical calculations illustrated that the N, P-doping at the edges of porous carbon structure with large surface area played a dominant role in achieving high electrocatalytic performance for ORR and OER. A Zn-air battery was assembled with NPCS coated carbon cloth as cathode, Zn plate as anode and polyacrylic acid as gel electrolyte. It displayed a specific capacity of 642 mAh/g_{zn} and long-term stability with no obvious voltage decay even when the battery was being bent to different angels. Chen *et al.* [82] developed N and S co-doped carbon textile (N, S-CC) by combining the carbothermic reaction and hydrothermal process. Benefiting from the dual-doping, this N, S-CC catalyst exhibited excellent electrochemical activity and durability for ORR and OER, even better than that of transition-metal catalysts. The potential of the N, S-CC electrode at 10 mA/cm^2 remains rather stable over 25,000 s in 1 mol/L KOH. N, S-CC without loading other materials yields a low ΔE value of 0.87 V in 1 mol/L KOH, outperforming the benchmark catalyst loaded CC such as Pt/C-CC and RuO_2-CC (1.10 and 1.02 V). The assembled flexible Zn-air battery coupled with zinc foil anode and alkaline gel electrolyte also demonstrated a stable charge/discharge capacity over 120 cycles at 5 mA/cm^2 under different bending conditions, and a higher power density than those of Pt/C and RuO_2.

Lee's group developed a 3D hybrid carbon nitride fiber network with high N content and P, S co-doping (denoted as PS-CNF), which offered an excellent catalytic ORR/OER performance and long-term durability with high mechanical strength for application in flexible Zn-air batteries [83]. They first prepared a stable polymeric C-N network *via* polymerizaiton at 300 °C (Fig. 3a) which was used for the *in situ* growth of a three-dimensional structure of P and S co-doped C-N nanofibers. The assembled flexible all-solid-state Zn-air battery with Zn foil anode and alkaline PVA gel polymer electrolyte exhibited excellent flexibility and cycling durability even when being bent to different angles (Figs. 3b and c). There was no obvious voltage difference before and after being bent to 120° for 100 cycles

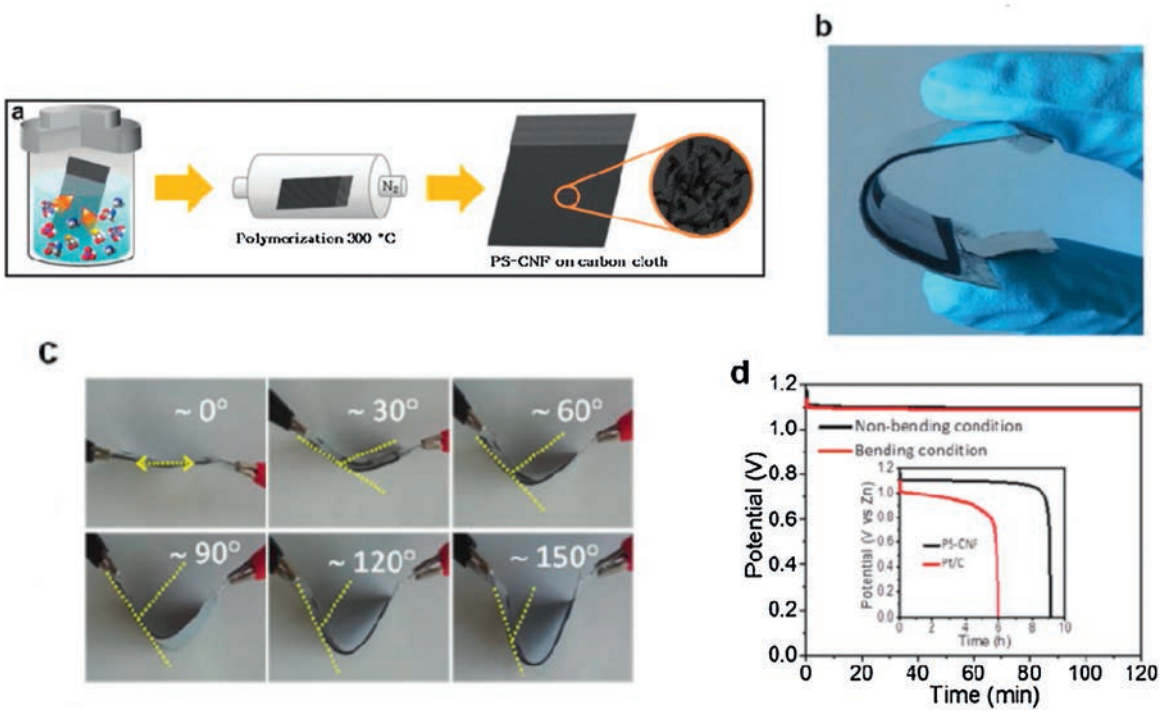

Fig. 3. (a) Schematic illustration of the in-situ fabrication process of P,S-CNF on carbon cloth. (b) Optical image of the prototype flexible Zn-air battery (ZAB) with P,S-CNF air electrodes. (c) Digital photographs of flexible ZABs upon being bent to various angles. (d) Discharge curves of flexible ZAB with PS-CNF under different bent conditions. Inset: Discharge curves of PS-CNF and Pt/C air electrodes in flexible ZABs. Adapted with permission [49]. Copyright 2017, the Royal Society of Chemistry.

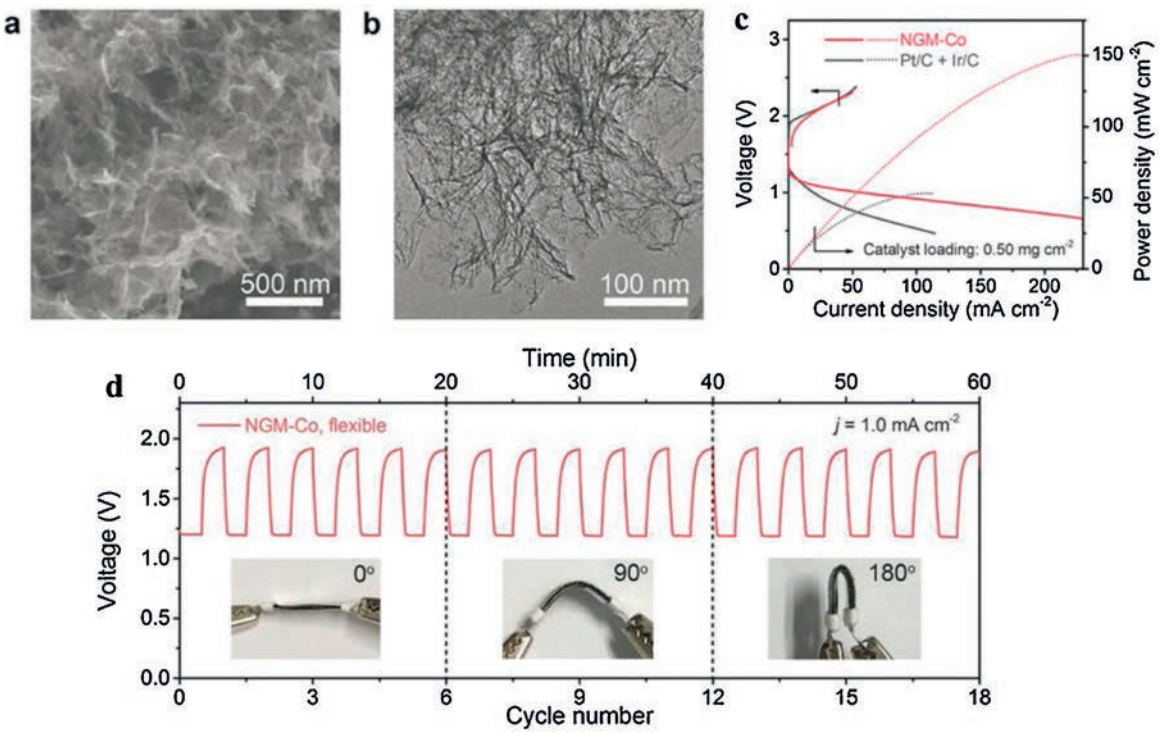

Fig. 4. (a) SEM image and (b) TEM image of NGM-Co catalyst. (c) Charge and discharge curves of NGM-Co based electrode in rechargeable solid Zn-air battery. (d) Galvanostatic discharge–charge cycling curves of flexible Zn-air battery under different bending. Adapted with permission [54]. Copyright 2017, John Wiley and Sons.

under a discharge current of 2 mA/cm^2 (Fig. 3d). Remarkably, P,S-CNF electrode showed excellent performance, a longer discharge time of ~9 h and a higher voltage plateau of ~1.1 V, compared to that 6 h discharge time and 1.0 V voltage plateau for Pt/C electrode. They also mentioned that this Zn-air battery had a relatively low discharge voltage compared to conventional liquid Zn-air battery, owing to the high contact resistance and poor ionic conductivity of PVA polymer gel.

2.2. Metal-nitrogen moieties doped carbon materials

In addition to the above mentioned non-metal-heteroatom-doped carbon materials, metal-nitrogen moieties-doped carbon materials (M-N-C) have also demonstrated significantly improved electrochemical performance in flexible Zn-air batteries [21,84–86]. Metal-nitrogen moieties-doped carbon materials (M-N-C) formed by introducing nitrogen atoms into the carbon materials and coordinating with metal atoms can enhance the interaction between metal species and carbon materials during ORR and OER [85]. The metal-nitrogen coordination structure with high-valent metal ions plays the key role in catalyzing oxygen reactions. This type of structure within a conductive and porous carbon matrix allows the accommodating of rich active sites as well as promotes the charge and mass transfer. Carbon material as the catalyst support could facilitate electron transfer and enable the flexibility for metal-nitrogen catalysts owing to its excellent electrical conductivity network and flexible nature. M-N-C structural defects induced by heteroatoms nitrogen doping on edges of carbon materials are reported to be favorable anchoring sites for metal atom due to the varied electron distribution on the defect site atoms [87]. Du *et al.* [85] designed N and Mo co-doped graphene (Mo-N-C) which exhibited a small potential difference of 0.8 V between the ORR half-wave potential ($E_{1/2}$) and OER potential at 10 mA/cm^2 (E_j = 10) in the same 0.1 mol/L KOH solution, which is even smaller than that of the Pt/C-IrO_2 combination. The great bifunctional ORR and OER electrocatalytic performance of Mo-N-C can be considered as the result of the more equidistant distribution of the free energy in each individual charge transfer step of the whole reaction sequence. Zhang *et al.* [86] fabricated three-dimensional (3D) bifunctional electrocatalyst which composited by CoNi alloy nanoparticle and carbon nanotube decorated N-doped carbon nanosheet arrays on carbon cloth (CoNi alloy/NCNSAs) *via* pyrolyzing polymetallic organic frameworks. This material exhibited superior ORR and OER electrocatalytic activities, such as a smaller potential difference of 0.676 V between OER and ORR half-wave potential, which is ascribed to the 3D hierarchical nanostructure promoted the mass transport, the higher graphitization facilitated the electronic mobility and the evenly dispersed active sites accelerated the kinetic reactions.

Tang *et al.* [54] prepared Co/N/O tri-doped graphene mesh (denoted as NGM-Co) *via* direct carbonization of the mixture of melamine, cobalt nitrate, gelatinized amylopectin and $Mg(OH)_2$. During the preparation, gelatinized amylopectin was carbonized to form few-layered graphene flakes and in-plane nanoholes after the removal of MgO template. They utilized the intrinsic structural defects in graphene sheets to generate the Co-N_x-C catalyst with a hierarchical porous structure and highly active sites for catalytic reaction. Such NGM-Co electrodes exhibited impressive electrocatalytic activities to oxygen reduction reactions and high flexibility. It could deliver a maximum power density of 152 mW/cm^2, a stable discharge voltage around 1.12 V at 20.0 mA/cm^2, a high energy efficiency of 63% at 1.0 mA/cm^2, and a small charge/discharge voltage gap of 0.7 V under different bending angles (Fig. 4). This outstanding Zn-air battery performance was ascribed to the abundant hierarchical porous structure

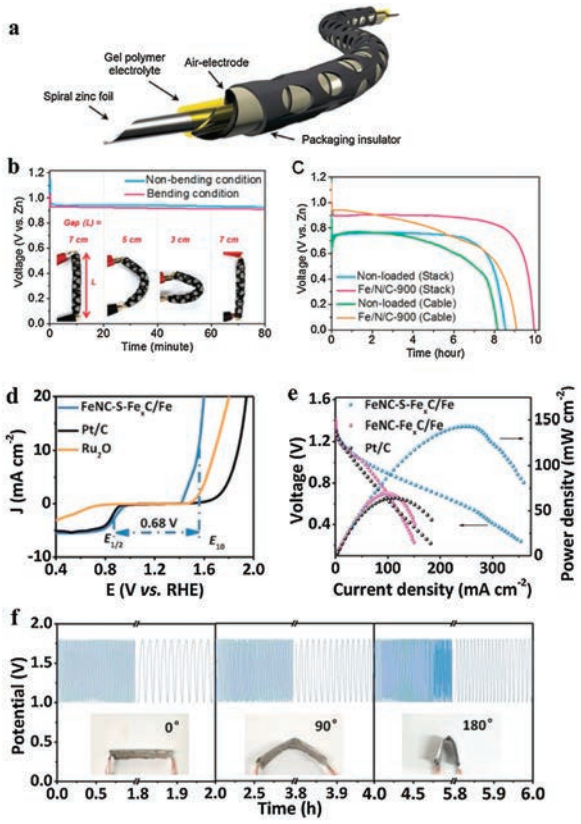

Fig. 5. (a) Schematic of a flexible cable-type Zn-air battery. (b) Discharge curves of cable-type Zn-air battery by applying bending strain. (c) Discharge curves of stack-type and cable-type Zn-air battery with and without Fe/N/C electrocatalysts. Adapted with permission [21]. Copyright 2014, John Wiley and Sons. (d) Linear sweep voltammetry (LSV) curves of FeNC-Fe_xC/Fe, Ru_2O and Pt/C catalysts for both ORR and OER. (e) Polarization and power density curves of the liquid Zn-air batteries using different catalysts. (f) Galvanostatic discharge–charge cycling curves for all-solid-state rechargeable Zn-air batteries under different bending strains. Adapted with permission [84]. Copyright 2018, John Wiley and Sons.

between NGM-Co sheets. The structural hierarchy together with an improved surface hydrophilicity favored the mass transfer in the catalytic reaction. Moreover, the abundant defective edges in graphene sheets facilitated the coordination of cobalt atoms with pyridinic N, resulting in the generation of highly dispersed Co-N_x-C species. Consequently, the charge distribution on the sp^2-conjugated carbon matrix was effectively modified by Co-N_x-C and oxygen functional group towards the optimal chemisorption of intermediates, which facilitated electron transfer leading to greatly improved catalytic activities to ORR. However, their effect on the OER activity was limited [81].

Meng *et al.* [88] introduced Co_4N/CNW/CC catalysts containing active sites of metallic Co_4N in combination with Co-N-C onto carbon fibers network of carbon cloth building a highly efficient bifunctional ORR/OER electrode for flexible Zn-air battery. This material could harness the advantages of superior OER activity from Co_4N and superior ORR activity from Co-N-C. Co_4N overcame the intrinsically low electrical conductivity of semiconducting Co-based oxides [89], and the transition metal in coordination with N created active sites for ORR. Similar as Co, the transition metal Fe coordinated with N atom demonstrated a promising catalytic ability to ORR as well, as it could effectively optimize the ORR intermediate adsorption [90,91]. In 2015 Cho's group first

fabricated an all-solid-state cable-type flexible Zn-air battery with an air electrode based on Fe/N/C electrocatalyst, a zinc foil anode and gel polymer electrolyte (Fig. 5a) [21]. The Fe/N/C catalyst was prepared by pyrolyzing the precursor composed of iron acetylacetonate, Ketjen black and silk fibroin. During the battery bending test at 0.1 mA/cm^2, no obvious changes were observed in the discharge voltage profiles under different bending conditions (Fig. 5b). The discharge curves of Zn-air battery based on Fe/N/C nonloaded and loaded air electrodes were shown in Fig. 5c. The Fe/N/C loaded air electrode demonstrated higher voltage plateau and longer duration time than the nonloaded in either stack-type or cable-type Zn-air batteries, which indicates that this type of Fe/N/C electrode was suitable for the use in flexible Zn-air batteries.

It was reported that iron-carbide-containing iron clusters (Fe_xC/Fe) may also be formed accompanied with the preparation of Fe/N/C during the pyrolysis [92]. The reduced Fe species as effective catalytic centers for ORR improved the catalytic efficiency of Fe/N/C systems [93]. Another method of promoting the electrocatalytic activity of an Fe/N/C system is to introduce electron-negative elements into carbon-based catalysts (*e.g.*, sulfur) [94]. Qiao *et al.* [84] introduced Fe-S bonds into the Fe/N/S system forming FeNC-S-Fe_xC/Fe catalyst in order to enhance the ORR activity, which was formed by pyrolyzing the mixture of polyaniline nanofibers and zeolitic imidazolate framework with sulfur power. The theoretical calculations and control experiments showed that the original Fe/N_x active centers could be enhanced by the formed Fe_xC/Fe clusters and C–S–C and Fe–S bonds. Accordingly, the FeNC-S-Fe_xC/Fe catalysts exhibited outstanding ORR/OER activity and durability in acidic electrolyte. In addition, FeNC-S-Fe_xC/Fe also showed smaller potential difference (0.68 V) between the ORR $E_{1/2}$ and the OER E_{10} than that of Pt/C and Ru_2O even in an alkaline medium (Fig. 5d). In liquid Zn-air battery, FeNC-S-Fe_xC/Fe showed higher power density and higher open-circuit voltage than that of Zn-air batteries with FeNC-Fe_xC/Fe and Pt/C catalysts (Fig. 5e). For flexible Zn-air battery, such electrodes demonstrated excellent electrocatalytic activity for Zn-air batteries, and outstanding stability under different bending angles as evidenced by minimal voltage changes during the bending tests (Fig. 5f).

3. Metal oxide and composites

Metal-based materials are considered as promising electrocatalysts with remarkable performance in metal-air batteries due to their conspicuous advantages including good fatigue resistance, high electrical conductivity and electro-oxidation stabilities. For Zn-air batteries, different kinds of metal materials have attracted attention spanning from noble metals (Pt, Ru, Pd) to rare earth metals (La, Yb, Ce) and transition metals (Ni, Co, Mn, Fe) [30,56,95]. For flexible electrocatalysis electrodes, a variety of metal-based materials have been reported. They include metal alloys (NiCo, FeCo), metal oxides (spinels, perovskites, rutile), metal hydroxides, metal nitrides, metal phosphides, metal organic framework materials, and metal-doped materials [56,95–100]. Most of the metals have more than one valence, and the electron transfer between different valence states form redox couples during ORR and OER [23]. The electrocatalytic activity can be controlled by adjusting the chemical constitution, crystal structure and oxidation state of metal oxides.

Transition-metal oxides (TMOs), in particular those mixed oxide varieties, possess the attributes of rich redox chemistry, relative abundance and low cost. They have demonstrated great potential as oxygen catalysts for energy storage and conversion [101–105]. Transition metal oxides are excellent oxygen-related catalysts in which the binding of adsorbents to metal cations (M) is neither too strong nor too weak [106]. With overall understanding of crystal structure for common transition metal oxides, it has confirmed that the [MO_6] octahedral configuration can effectively accelerate the charge transfer process during a redox reaction [107]. In the octahedral field, the 3d orbit of transition metal is split into e_g and t_{2g}. It thereof determines the energy gained by both the adsorption/desorption of oxygen on transition metal ions [108]. In order to achieve enhanced electrocatalytic ability to oxygen, different methods have been developed to tailor the electronic structure of metal active sites, including surface modification, structural adjustment and element doping [20,32,33,56,95,109–111]. Jiang and co-workers fabricated an ultrathin one nanometer CoO_x supported on metallic Co/N-doped graphene substrate (CoO_x/N-RGO) by a simple ligand-assisted calcination method [112]. The ultrathin CoO_x layer structure not only provided abundant active sites and accelerated electron conduction, but also facilitated electron

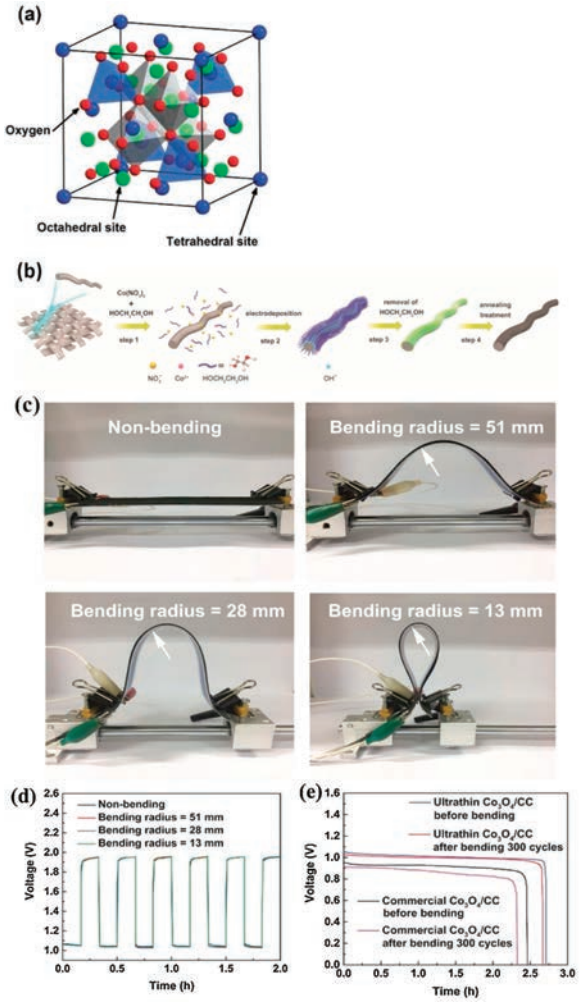

Fig. 6. (a) The model of spinel crystal structure. Adapted with permission [107]. Copyright 2017, Wiley-VCH. (b) Schematic diagram of the preparation procedure of flexible air electrode. (c) Optical photographs of integrated devices consisting of a flexible Zn–air battery and a flexible display unit under various bending radii. (d) Galvanostatic discharge and charge testing of flexible Zn-air battery under various bending radii. (e) Discharge performance of flexible Zn-air batteries using ultrathin Co_3O_4/CC electrode and commercial ultrathin Co_3O_4/CC air electrodes before and after the repeated bending at a bending radius of 28 mm for 300 cycles. Adapted with permission [20]. Copyright 2017, John Wiley and Sons.

transfer with Co/N-doped graphene, resulting in excellent oxygen electrocatalytic performance. Moreover, at the atomic scale, ultrathin CoO_x exhibited the advantages of ultrahigh flexibility, cycling stability and lightweight, which are the most desirable merits for wearable electronic devices.

Spinel and perovskite oxides are transition metal oxides with special crystal structures and abundance oxygen vacancy that offer excellent catalytic activity [16,107], and they have been extensively investigated as bifunctional electrocatalysts for ORR and OER in Zn-air batteries. Spinel oxides can be synthesized by simple method with stable catalytic performance, and have low cost and multi-oxidation states. As for spinel oxides, perovskite oxides have also gained attention in the area of oxygen electrocatalysis owing to their earth-abundant elements, thermal stability, structural flexibility and excellent electrocatalytic performance [95,100]. Therefore, this minireview will highlight the recent progress on flexible metal oxides-based electrodes for Zn-air batteries and mainly focus on spinel, perovskite oxides and their composites.

3.1. Spinel oxides and composites

Spinel oxides are generally expressed in a formula of AB_2O_4 (A: Mg, Ni, Fe, Co, Mn, *etc.*; B: Al, Fe, Co, Cr, Mn, Ni, *etc.*), in which oxygen anions are in the form of cubic close packing, 1/8 of the tetrahedral sites are occupied by A atom, whereas 1/2 of the octahedral sites are occupied by B atom (Fig. 6a) [107]. Spinel oxides with mixed valences exhibit electrical and semiconducting properties which allow them to be used directly as electrocatalysts, and the transfer of electrons can occur at relatively low activation energy [107]. Spinel oxides as bifunctional oxygen electrocatalysts for Zn-air batteries have demonstrated excellent discharging/charging performance and stability [56,113]. For wearable Zn-air batteries, flexible air electrodes can be designed *via* changing the construction and composition of spinel oxides. Di and Li [49] utilized lightweight conductive nitrogen-doped carbon nanotubes as substrate for loading cobalt oxides nanoparticles (Co_3O_4/N-CNT), in order to provide more channel for gas diffusion and improve the electrocatalytic activity for ORR and OER. The solid-state Zn-air battery assembled with Co_3O_4/N-CNT aerogel films exhibited a long-term stable open-circuit potential, as revealed by the negligible change for charge transfer resistance upon a 90° bending. However, they did not discuss the battery performance regarding to the energy density and power density. Zhong and co-workers [20] first developed an integrated electronic device, consisting of a flexible Zn-air battery integrated with a flexible display device. The assembled flexible Zn-air battery composed of Cu deposited Zn anode, spinel Co_3O_4/CC air electrode, and hydrogel electrolyte. The preparation procedure of the Co_3O_4/CC flexible air electrode is shown in Fig. 6b. $Co(OH)_2$ was grown *in situ* on the surface of carbon fibers in carbon cloth by electrodeposition, then Co_3O_4/CC was formed upon annealing at 400 °C in air. In this work, Zn-air batteries did not exhibit obviously changed galvanostatic charge/discharge behaviours under various bending radii of 0, 13, 28 and 51 mm (Figs. 6c and d), also no obvious change in the discharge performance before and after being repeatedly bent at a bending radius of 28 mm for 300 cycles either (Fig. 6e). Such high mechanical stability and excellent rechargeable performance of Co_3O_4/CC air electrode could be ascribed to the strong adhesion of Co_3O_4 on conductive CC support. Ji *et al.* [32] introduced rich oxygen vacancies into Co_3O_4 particles by regulating the oxidation process under relatively low-temperature on the basis of Kirkendall effect. They also introduced a porous N-doped carbon structure to Co_3O_4 and obtained Co_3O_{4-x} HoNPs@HPNCS-60, to improve the electrocatalytic activity and flexibility of Co_3O_4. With tailored oxygen vacancies as well as the unique structure design, this electro-catalyst exhibited a higher discharge potential (*ca.* 1.2 V) as well as a lower charge potential (*ca.* 1.73 V) than those of commercial Pt/C + RuO_2 catalysts (*ca.* 1.18 V and 1.90 V, respectively). This battery offered a high capacity of 779.36 mAh/g_{zn} with a power density of 94.1 mW/cm^2. The assembled Zn-air batteries could light 8 yellow lights and exhibited a stable cycle performance.

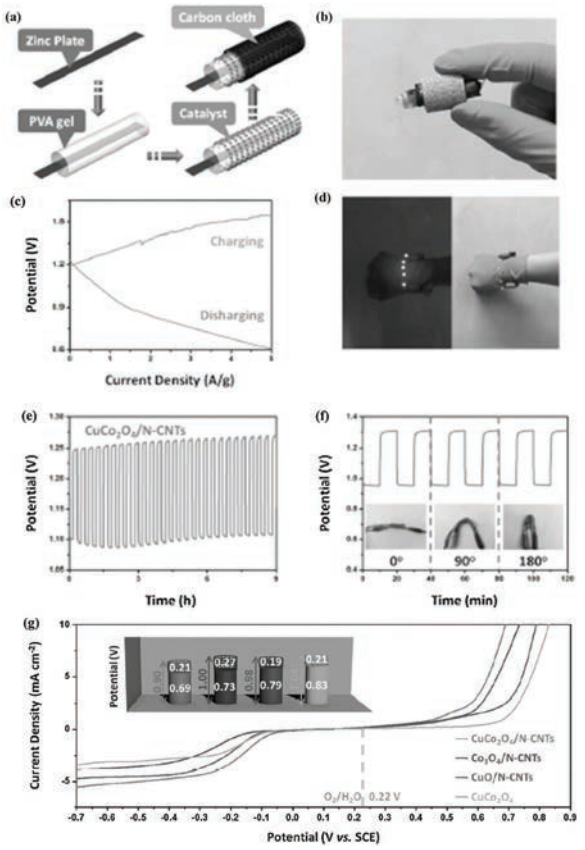

Fig. 7. (a) Schematic illustration of the fabrication and structure of flexible Zn-air battery. (b) Configuration of the Zn-air battery with $CuCo_2O_4$/N-CNTs air cathode. (c) Charging and discharging polarization curves. (d) Photograph of five blue LEDs powered by two Zn-air batteries in series. (e) Charging and discharging profiles at a current density of 0.5 A/g. (f) Charging and discharging curves at a current density of 1 A/g under different bending angles. (g) Linear-sweep curves of $CuCo_2O_4$/N-CNTs, Co_3O_4/N-CNTs, CuO/N-CNTs, and $CuCo_2O_4$ in O_2 saturated 0.1 mol/L KOH solution at scan rate of 10 mV/s. Adapted with permission [56]. Copyright 2017, John Wiley and Sons.

Liu's group [56] also reported a flexible all-solid-state Zn-air battery composed of spinel $CuCo_2O_4$ air cathode in a bracelet configuration, which could be worn on the hand and power blue LED. This flexible battery system showed a constant charge (1.29 V) and discharge (0.98 V) platforms at a current density of 1 A/g, even when it was bent to 90° or 180° (Fig. 7). They also concluded that the electrocatalytic activity of $CuCo_2O_4$ was improved because of the synergetic effect between $CuCo_2O_4$ and N-doped carbon nanotubes. The Co_3O_4/ N-CNTs showed worse ORR activities than CuO/N-CNTs, indicating that CuO had greater ORR catalytic activities than Co_3O_4. Meanwhile, the doping of Cu into Co_3O_4 promoted the ORR activities of Co_3O_4 due to the new active sites created by the Cu doping (Fig. 7g).

Zeng *et al.* [114] and Ge *et al.* [30] assembled flexible and stretchable Zn-air batteries with spinel $NiCo_2O_4$ as the electrocatalyst of air cathode. The Zn-air batteries still functioned well and lightened red LEDs when the batteries were being folded,

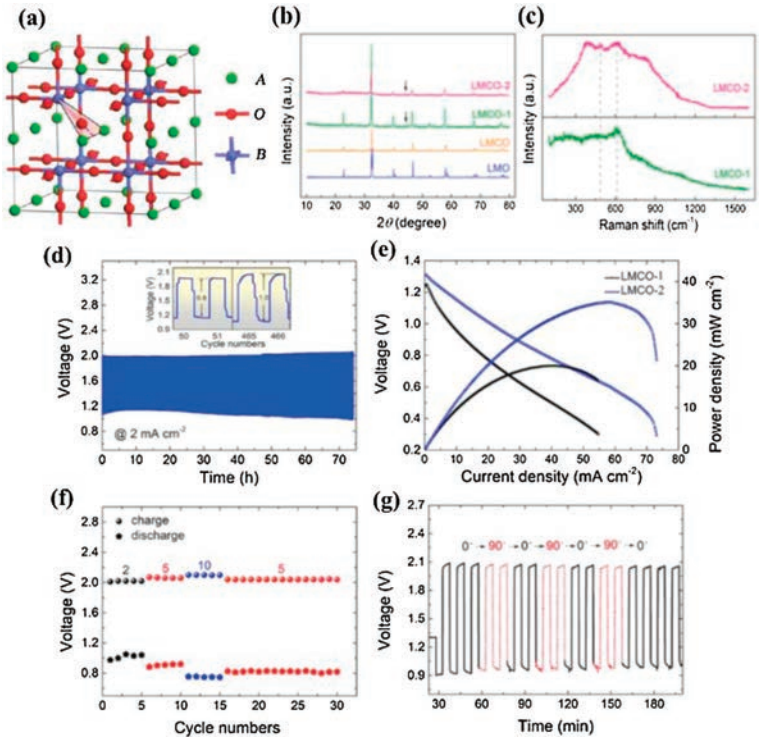

Fig. 8. (a) The model of perovskite oxides. (b) XRD patterns of different LMCO. (c) Raman spectra of different LMCO. (d) Long-term cycling performance of flexible Zn-air battery with LMCO-2 catalyst. (e) Discharging polarization curves of flexible Zn-air battery with LMCO-1 and LMCO-2 catalysts. (f) Cycling performance of flexible Zn-air battery with LMCO-2 catalyst at different current densities. (g) Discharge/charge cycling curves of flexible ZABs with LMCO-2 cathode under different bending conditions. (a) Adapted with permission [117]. Copyright 2010, Elsevier. (b-g) Adapted with permission [95]. Copyright 2019, American Chemical Society.

twisted to spiral shape, or wavy bended, all suggesting the high flexibility and high mechanical strength. In addition, the Zn-air battery using spinel $NiCo_2O_4$ as electrocatalyst displayed a low overpotential, a high energy density (954.2 Wh/kg), a high capacity (826.9 mAh/g) and long term stability (600 cycles at 5 mA/cm^2), which were superior to that of commercial Pt/C + Ir/C catalyst [115]. Therefore, spinel oxide-based air cathodes are considered as promising materials for next-generation flexible and wearable Zn-air batteries.

3.2. Perovskite oxide and composites

For perovskite-type oxides the general formula can be expressed as ABO_3 (A: alkaline earth or rare-earth metal with 12-fold oxygen coordination; B: a transition metal with six-fold oxygen coordination) (Fig. 8a). By partial substitution of cations at A or B, or both A and B sites, a variety of perovskite oxides can be obtained with a formula of AA'BB'O_3 and offer a "soft" nature of physicochemical properties [116,117]. By virtue of this unique structure, perovskite oxides can be used as bifunctional electrocatalysts for flexible Zn-air batteries. Bian *et al.* [95] reported the perovskite $LaMn_{0.75}Co_{0.25}O_{3-\delta}$ (LMCO) catalyst for Zn-air battery. They first doped reducible Co at the B site of perovskite $LaMnO_3$ under the 5% H_2-Ar atmosphere to enable the uniform distribution of cobalt nanoparticles on the surface of perovskite nanofibers as well as produce more oxygen vacancies. The XRD spectra show the phase structure indexed to the $LaMnO_3$ phase and metallic Co (Fig. 8b). The Raman spectra (peaks: 490 and 610 cm^{-1}) indicated the forming of oxygen valences in LMCO-2 rather than LMCO-1 catalysts (Fig. 8c). The assembled Zn-air battery with zinc foil anode and alkaline electrolyte exhibited excellent flexibility under repeated bending between 90° and 0°, but delivered a relatively low power density of 35 mW/cm^2 and a limited cycling stability of 70 h (Figs. 8e–g). The results from electron energy loss spectroscopy confirmed that the electrochemical performance of this perovskite material as an electrocatalyst for oxygen redox reaction was ascribed to the abundant oxygen vacancies and lager number of metal ions in a high oxidation state. The Zn-air battery assembled with $LaMn_{0.75}Co_{0.25}O_{3-\delta}$ air electrode and Zn foil anode demonstrated excellent flexibility, but its power density was too low to be applied as a power source. Yang *et al.* [118] prepared perovskite lanthanum nickel oxide/nitrogen doped carbon nanotubes ($LaNiO_3$/NCT), and then coated onto carbon cloth for use as flexible air cathode. The assembled flexible Zn-air battery with zinc film anode and poly vinyl alcohol (PVA) gelled electrolyte exhibited superior rechargeability and performance durability over 120 cycles at a constant charge-discharge current density of 50 A/kg without losing the performance even under different bending angles. Moreover, this battery showed a high energy density of 581 Wh/kg, which could meet the needs of wearable and portable electronic devices. The derived superior flexibility and performance can be attributed to the highly flexible electrodes and excellent electrocatalytic activity of $LaNiO_3$/NCT catalyst.

In summary, the electrochemical activity and flexibility of some selected bifunctional materials for flexible Zn-air batteries are shown in Table 1 [20,21,28,30,32,49,50,54,56,82-86,88,95,112,118–120].

4. Conclusion and perspectives

To meet the growing energy demands for flexible/wearable electronic devices, the driving power sources are required to possess the merits of intrinsic safety, high energy and power densities, and low self-discharge. Flexible Zn-air batteries are

Table 1
Electrochemical activity and flexibility of bifunctional materials for flexible Zn-air batteries from recent reports.

Catalysts	Bifunctional material	Stability	Electrocatalytic performance (Specific capacity, energy/ power density)	Flexibility evaluation	Ref
	P,S co-doped on carbon nitride fibers	240 h of stable operation.	698 mAh/g; 785 Wh/kg.	100 cycles at 2 mA/g at a bending angles of 120°.	[83]
	B-doped graphene quantum dots on a graphene hydrogel	Stable discharge voltage of 1.23 V for 100 h.	687 mAh/g; 112 mW/cm^2.	Stable charge (2.01 V) and discharge potentials (1.18 V) at 10 mA/cm^2 for 15 h under different bending angles.	[119]
Heteroatom-doped carbons	N,P co-doped carbon spheres	Discharge/charge process could be well-maintained for 30 h.	55 mW/cm^2; 642 mAh/g.	No obvious potential decay under bending at various angels.	[28]
	N,S co-doped carbon skeleton	Stable long cycle life over 1000 cycles.	715 mAh/g_{Zn}; 829 Wh/kg_{Zn}.	Charge/discharge potentials were maintained 120 cycles at 5 mA/cm^3 under different bending conditions.	[82]
	nanoporous carbon nanofiber film	After 500 cycles (about 83 h), a slight performance loss.	185 mW/cm^2; 776 Wh/kg.	Stable charge and discharge potentials for 6 h under bending or folding back and forth.	[50]
	S doped Fe-N-C species	Higher voltage plateau of 1.35 V for about 13,800 s at 2 mA/cm^2.	Overpotential: 1.00 V at 100 mA/cm^2; 740.8 mAh/g_{Zn}.	Curled Zn-air battery displayed a long lifetime.	[120]
	graphene with both N and Mo dopants	Stable voltage over the 88 h test.	83 mW/cm^2; The voltage gap between discharge and charge is ~0.77 V at 2 mA/cm^2.	Discharge/charge voltage remained unchanged under different bending conditions.	[85]
Metal-nitrogen moieties doped carbon materials	CoNi alloy and carbon nanotube decorated N-doped carbon nanosheet arrays	Stable performance after the 800-min cycles.	98.8 mW/cm^2; 879 mA h/g.	Discharge/charge voltage remained unchanged when being bent to 90° and 180°.	[86]
	N-doped carbon species anchor Co_4N particles and Co-N-C active sites on intertwined N-C fibers	No visible change after continuous cycling of more than 136 h (up to 408 cycles).	Open-circuit voltage: 1.346 V; 774 mAh/g.	After 2000 cycles of bending/stretching, voltage of the discharge only drop of 13 mV.	[88]
	Co/N/O tri-doped graphene mesh	Stable discharge voltage for more than 60 h.	Open-circuit voltage: 1.44 V; 152 mW/cm^2.	A small charge/discharge voltage gap of 0.7 V under different bending angles (0°, 90°, 180°).	[54]
	Fe/nitrogen/carbon	Voltage plateau 0.9 V during 10 h discharge times.	Open cell voltage: 2.97 V.	No differences in the discharge voltage profiles between the bending and non-bending conditions.	[21]
	FeNC–S–Fe_xC/Fe	Activity did not decay even after 10,000 cycles.	Open-circuit voltage: 1.41 V; Charge–discharge voltage gap: 0.9 V at 2 mA/cm^2; 149.4 mW/cm^2.	Stable charge (1.8 V) and discharge (1.0 V) potentials for 6 h even when folded to different angles (0°, 90°, 180°).	[84]
	CoO_x on Co/N-doped graphene substrate.	No apparent changes in the charge/discharge potentials at 6 mA/cm^2, after 10 h cycling.	300 W/g_{cat}; Open-circuit voltage: 1.39 V.	Stable charge (1.82 V) and discharge (1.25 V) potentials when being bent from 0° to 180°.	[112]
	cobalt(II/III) oxide/nitrogen-doped CNT	Stable charging and discharging potentials for 20 h at 2 mA/cm^2.	A red light emitting diode was powered up by two flexible batteries in series for hours; Battery ohmic resistance: 5 Ω	Stable open-circuit potential when the battery is folding.	[49]
Metal oxide and composites	Co_3O_4 layers on the surface of carbon fibers in the carbon cloth	Stable discharge performance at a bending radius of 28 mm for 300 cycles.	Discharge voltage: 1.03 V, charge voltage: 1.95 V at 2 mA/cm^2; Energy density: 546 Wh/kg.	Not obviously changed in the charge/ discharge behaviours under various bending radii of 0, 13, 28 and 51 mm.	[20]
	Co_3O_{4-x} hollow nanoparticles with hierarchically porous N-doped carbon structure (HPNCS)	A slight increasing charging–discharging potential gap after 50 cycles.	779.36 mAh/g_{zn}; 94.1 mW/cm^2.	N/A	[32]
	nitrogen-doped carbon nanotubes decorated by $CuCo_2O_4$	Stable rechargeability with low charging voltages under a constant current density of 0.5 A/g.	1.86 W/g, Five blue LED powered by two Zn–air batteries connected in series.	Unchanged constant charging (1.29 V) and discharging (0.98 V) platforms when bent to different angles (0°, 90°, 180°).	[56]
	$NiCo_2O_4$/N-doped carbon nanowebs	Stable voltage gap of 0.80 V during 40 h at a 5 mA/cm^2.	826.9 mAh/g; 954.2Wh/kg.	Photograph showed the bendability.	[30]
	$LaMn_{0.75}Co_{0.25}O_{3-\delta}$ nanofiber	Cycle steadily for 70 h with little voltage change at 2 mA/cm^2	35 mW/cm^2.	No obvious polarization under repeatedly bending between 90° and 0°.	[95]
	Lanthanum nickel oxide/ nitrogen doped carbon nanotubes	Stable 120 cycles test at 250 A/L (50 A/kg).	581 Wh/kg.	Wearable prototype integrated with a tandem device in series to power a LED under bent condition.	[118]

considered as one of the most promising candidates, but have not yet penetrated the commercial market owing to their low practical energy density, mechanical performance and stability, which are all closely related to air electrodes. This minireview presents the recent progress in flexible air electrodes with bifunctional electrocatalysts. We highlight the latest innovations in two commonly used catalysts for flexible Zn-air batteries: carbon based and metal oxide materials.

Combining N with other heteroatoms, like P or S forming co-doped or tri-doped carbon can further change the surface

electronic states and polarities of carbon atoms for improved electrochemical ORR and OER performance. These materials have demonstrated excellent electrocatalytic activity and long-term cycle performance in Zn-air batteries owing to the synergistic electronic interactions between different dopants and adjacent carbon atoms. Metal-nitrogen moieties doped carbons can offer high electrocatalytic activity and stability for ORR and OER, owing to the offering of more active sites and improved charge/mass transfer. These carbon-based air electrodes have demonstrated stable electrocatalytic performance in flexible Zn-air batteries during the deformation processes as well.

Transition-metal oxides, in particular mixed oxide varieties, have demonstrated the great potential as oxygen catalysts for energy storage and conversion. Transition metal oxides with perovskite or spinel crystal structure have been demonstrated as promising bifunctional catalysts for oxygen redox reactions in alkaline solutions. In addition to the downsizing and nano-structuring of metal oxides to improve the mass activity, their catalytic performance can also be significantly enhanced by modifying the surface electronic structure to yield high intrinsic activity.

It should be pointed out that currently there are still many technical challenges facing the development of flexible Zn-air batteries with excellent performance and mechanical flexibility.

First, it is to improve the low practical energy density, and the development of highly efficient electrode catalysts holds the key. For zinc anode, it needs to inhibit the formation of zinc dendrite and capacity loss during the charge-discharge cycles [15,43,121], which is beyond the scope of this review. For bifunctional oxygen electrocatalysts, their low practical energy density can be improved by creating a structure with more active sites and enhanced charge/mass transfer [27]. The morphology control is an effective method, and the desirable structures mainly include porous structure, hollow structure, core-shell structure, or hierarchical-structure constructed with 1D, 2D or 3D nanofeatures. Another issue is the robustness of the electrodes and the battery system. Namely, the high capacity and long cycling stability need to be maintained when they are being subjected to a deformation. The intrinsically flexible battery configuration can be achieved when each component satisfies the requirement of mechanical flexibility. In addition, the economic and environmental issue should be also considered during the development of bifunctional electrocatalyst.

Second, the evaluation standards of flexible batteries should be established in the aspects of electrochemical performance as well as the mechanical flexibility, such as the standard testing procedure to evaluate the flexibility during the folding, bending, and twisting tests.

Third, the fundamental research on the understanding of electrochemical processes and structural changes of materials is equally important in the development of flexible Zn-air batteries, which will promote the development of new materials with superior striking properties.

It can also be expected that the development of flexible and efficient bifunctional oxygen electrocatalysts for Zn-air batteries will provide useful information for other flexible metal-air batteries, as well as in the fields of fuel cells or water splitting.

Declaration of competing interest

The authors report no declarations of interest.

Acknowledgments

The authors thank the financial supports from the Science and Technology Program of Longyan (No. 2018LYF8010), the Natural Science Foundation of Fujian Province (No. 2019J01800), and the Qimai Natural Science Foundation of Shanghang County (No. 2018SHQM01). C. Wang acknowledges the funding from the Australian Research Council Centre of Excellence Scheme (No. CE 140100012).

References

[1] A. Nathan, A. Ahnood, M.T. Cole, et al., P. IEEE 100 (2012) 1486–1517.
[2] K. Takei, W. Honda, S. Harada, et al., Adv. Healthc. Mater. 4 (2015) 487–500.
[3] L. Li, Y. Bai, L. Li, et al., Adv. Mater. 29 (2017) 1702517.
[4] C. Wang, K. Xia, H. Wang, et al., Adv. Mater. 31 (2019) 1801072.
[5] H.M. Lee, S.Y. Choi, A. Jung, S.H. Ko, Angew. Chem. Int. Ed. 52 (2013) 7718–7723.
[6] D. Wang, Y. Zhang, X. Lu, et al., Chem. Soc. Rev. 47 (2018) 4611–4641.
[7] H. Kim, J.H. Ahn, Carbon 120 (2017) 244–257.
[8] F. Ning, Y. Shen, C. Bai, et al., Chin. Chem. Lett. 30 (2019) 1282–1288.
[9] L. Liu, Z. Niu, J. Chen, Chin. Chem. Lett. 29 (2018) 571–581.
[10] B. Li, S. Zhang, B. Wang, et al., Energy Environ. Sci. 11 (2018) 1723–1729.
[11] Y. Jiang, Y.P. Deng, R. Liang, et al., Adv. Energy Mater. 9 (2019) 1900911.
[12] Y. Zhao, Q. Lai, Y. Wang, et al., ACS Appl. Mater. Inter. 9 (2017) 16178–16186.
[13] V. Caramia, B. Bozzini, Mater. Renew. Sustain. Energy 3 (2014) 28–40.
[14] B. Chen, D.Y.C. Leung, J. Xuan, H. Wang, Appl. Energy 185 (2017) 1303–1308.
[15] Y. Li, H. Dai, Chem. Soc. Rev. 43 (2014) 5257–5275.
[16] J.S. Lee, S.T. Kim, R. Cao, et al., Adv. Energy Mater. 1 (2011) 34–50.
[17] C. Su, H. Cheng, W. Li, et al., Adv. Energy Mater. 7 (2017) 1602420.
[18] B.Y. Xia, Y. Yan, N. Li, et al., Nat. Energy 1 (2016) 1–6.
[19] G. Kannan, P. Sasikumar, K. Devika, Appl. Math. Model. 34 (2010) 655–670.
[20] X. Chen, B. Liu, C. Zhong, et al., Adv. Energy Mater. 7 (2017) 1700779.
[21] J. Park, M. Park, G. Nam, et al., Adv. Mater. 27 (2015) 1396–1401.
[22] S. Patra, R. Choudhary, E. Roy, et al., Nano Energy 30 (2016) 118–129.
[23] M. Prabu, P. Ramakrishnan, H. Nara, et al., ACS Appl. Mater. Inter. 6 (2014) 16545–16555.
[24] J. Pan, Y.Y. Xu, H. Yang, et al., Adv. Sci. 5 (2018) 1700691.
[25] J. Fu, Z.P. Cano, M.G. Park, et al., Adv. Mater. 29 (2017) 1604685.
[26] J.E.C. Sabisch, A. Anapolsky, G. Liu, A.M. Minor, Resour. Conserv. Recycl. 129 (2018) 129–134.
[27] P. Tan, B. Chen, H. Xu, et al., Energy Environ. Sci. 10 (2017) 2056–2080.
[28] S. Chen, L. Zhao, J. Ma, et al., Nano Energy 60 (2019) 536–544.
[29] A.M. El-Sawy, I.M. Mosa, D. Su, et al., Adv. Energy Mater. 6 (2016) 1501966.
[30] H. Ge, G. Li, T. Zheng, et al., Electrochim. Acta 319 (2019) 1–9.
[31] C. Hu, L. Dai, Adv. Mater. 29 (2017) 1604942.
[32] D. Ji, L. Fan, L. Tao, et al., Angew. Chem. Int. Ed. 58 (2019) 13840–13844.
[33] D. Ji, S. Peng, D. Safanama, et al., Chem. Mater. 29 (2017) 1665–1675.
[34] S. Li, X. Yang, S. Yang, et al., J. Mater. Chem. A 8 (2020) 5601–5611.
[35] C. Du, Y. Gao, J. Wang, W. Chen, J. Mater. Chem. A 8 (2020) 9981–9990.
[36] Y. Yan, Y. Xu, B. Zhao, et al., J. Mater. Chem. A 8 (2020) 5070–5077.
[37] K.N. Dinh, Z. Pei, Z. Yuan, et al., J. Mater. Chem. A 8 (2020) 7297–7308.
[38] J. Spendelow, A. Wieckowski, Phys. Chem. Chem. Phys. 9 (2007) 2654–2675.
[39] F. Jaouen, E. Proietti, M. Lefèvre, Energy Environ. Sci. 4 (2011) 114–130.
[40] K. Kinoshita, Electrochemical Oxygen Technology, John Wiley & Sons, California, 1992.
[41] X. Wang, P.J. Sebastian, M.A. Smit, et al., J. Power Sources 124 (2003) 278–284.
[42] X. Li, F. Dong, N. Xu, et al., ACS Appl. Mater. Interfaces 10 (2018) 15591–15601.
[43] J. Fu, R. Liang, G. Liu, et al., Adv. Mater. 31 (2019) 1805230.
[44] H.F. Wang, C. Tang, Q. Zhang, Adv. Funct. Mater. 28 (2018) 1803329.
[45] Y. He, B. Matthews, J. Wang, et al., J. Mater. Chem. A 6 (2018) 735–753.
[46] Q. Liu, Z. Chang, Z. Li, X. Zhang, Small Methods 2 (2018) 1700231.
[47] G. Zubi, R. Dufo-López, M. Carvalho, G. Pasaoglu, Renew. Sust. Energy Rev. 89 (2018) 292–308.
[48] Y. Xu, Y. Zhang, Z. Guo, et al., Angew. Chem. 127 (2015) 15610–15614.
[49] S. Zeng, H. Chen, H. Wang, et al., Small 13 (2017) 1700518.
[50] Q. Liu, Y. Wang, L. Dai, J. Yao, Adv. Mater. 28 (2016) 3000–3006.
[51] A.B.A. Reyimjan, A. Sidik, J. Phys. Chem. B 110 (2006) 1787–1793.
[52] X. Cai, L. Lai, J. Lin, Z. Shen, Mater. Horizons 4 (2017) 945–976.
[53] R. Paul, F. Du, L. Dai, et al., Adv. Mater. 31 (2019) 1805598.
[54] C. Tang, B. Wang, H.F. Wang, Q. Zhang, Adv. Mater. 29 (2017) 1703185.
[55] M. Zhang, L. Dai, Nano Energy 1 (2012) 514–517.
[56] H. Cheng, M.L. Li, C.Y. Su, et al., Adv. Funct. Mater. 27 (2017) 1701833.
[57] Y. Cheng, Y. Tian, X. Fan, et al., Electrochim. Acta 143 (2014) 291–296.
[58] X. Zheng, X. Cao, K. Zeng, et al., J. Mater. Chem. A 8 (2020) 11202–11209.
[59] K. Tang, C. Yuan, Y. Xiong, et al., Appl. Catal. B 260 (2020) 118209.
[60] G.L. Tian, M.Q. Zhao, D. Yu, et al., Small 10 (2014) 2251–2259.
[61] C. Zhu, S. Dong, Nanoscale 5 (2013) 1753–1767.
[62] J. Zhang, Z. Zhao, Z. Xia, L. Dai, Nat. Nanotechnol. 10 (2015) 444–452.
[63] K. Qu, Y. Zheng, S. Dai, S.Z. Qiao, Nano Energy 19 (2016) 373–381.
[64] C. Hu, L. Dai, Adv. Mater. 31 (2019) 1804672.
[65] Q. Lv, W. Si, J. He, et al., Nat. Commun. 9 (2018) 3376.
[66] C. Tang, H.F. Wang, X. Chen, et al., Adv. Mater. 28 (2016) 6845–6851.
[67] W. Lei, Y. Deng, G. Li, et al., ACS Catal. 8 (2018) 2464–2472.
[68] X. Liu, L. Dai, Nat. Rev. Mater. 1 (2016) 1–12.
[69] F.L. Meng, K.H. Liu, Y. Zhang, et al., Small 14 (2018) 1703843.
[70] J. Zhang, L. Dai, Angew. Chem. Int. Ed. 55 (2016) 13296–13300.

[71] Z. Lu, J. Wang, S. Huang, et al., Nano Energy 42 (2017) 334–340.
[72] Y. Qian, Z. Hu, X. Ge, et al., Carbon 111 (2017) 641–650.
[73] X. Zheng, X. Cao, J. Wu, et al., Carbon 107 (2016) 907–916.
[74] W. Schofberger, F. Faschinger, S. Chattopadhyay, et al., Angew. Chem. Int. Ed. 55 (2016) 2350–2355.
[75] W. Zhang, W. Lai, R. Cao, Chem. Rev. 117 (2017) 3717–3797.
[76] Z.W. Seh, J. Kibsgaard, C.F. Dickens, et al., Science 146 (2017) 4998.
[77] H.W. Liang, X. Zhuang, S. Bruller, et al., Nat. Commun. 5 (2014) 4973.
[78] H. Zhang, R. Lv, J. Materiomics 4 (2018) 95–107.
[79] T.Y. Ma, J. Ran, S. Dai, et al., Angew. Chem. 54 (2015) 4646–4650.
[80] Y. Zhao, R. Nakamura, K. Kamiya, et al., Nat. Commun. 4 (2013) 2390.
[81] S. Chen, J. Duan, M. Jaroniec, S.Z. Qiao, Adv. Mater. 26 (2014) 2925–2930.
[82] Z. Zhao, Z. Yuan, Z. Fang, et al., Adv. Sci. 5 (2018) 1800760.
[83] S.S. Shinde, J.Y. Yu, J.W. Song, et al., Nanoscale Horizons 2 (2017) 333–341.
[84] Y. Qiao, P. Yuan, Y. Hu, et al., Adv. Mater. 30 (2018) 1804504.
[85] P. Du, K. Hu, J. Lyu, et al., Appl. Catal. B 276 (2020) 119172.
[86] W. Zhang, Z. Li, J. Chen, et al., Nanotechnology 31 (2020) 185703.
[87] Y. Ito, T. Ohto, D. Hojo, et al., ACS Catal. 8 (2018) 3579–3586.
[88] F. Meng, H. Zhong, D. Bao, et al., J. Am. Chem. Soc. 138 (2016) 10226–10231.
[89] P. Chen, K. Xu, Z. Fang, et al., Angew. Chem. 54 (2015) 14710–14714.
[90] W.J. Jiang, L. Gu, L. Li, et al., J. Am. Chem. Soc. 138 (2016) 3570–3578.
[91] A. Kudo, Y. Miseki, Chem. Soc. Rev. 38 (2009) 253–278.
[92] U.I. Kramm, I. Herrmann-Geppert, J. Behrends, et al., J. Am. Chem. Soc. 138 (2016) 635–640.
[93] J.A. Varnell, E.C. Tse, C.E. Schulz, et al., Nat. Commun. 7 (2016) 12582.
[94] Q. Li, W. Chen, H. Xiao, et al., Adv. Mater. 30 (2018) e1800588.
[95] J. Bian, Z. Li, N. Li, C. Sun, Inorg. Chem. 58 (2019) 8208–8214.
[96] D. Ji, L. Fan, L. Li, et al., Adv. Mater. 31 (2019) e1808267.
[97] H. Zhang, T. Wang, A. Sumboja, et al., Adv. Funct. Mater. 28 (2018) 1804846.
[98] Y. Li, J. Yin, L. An, et al., Nanoscale 10 (2018) 6581–6588.
[99] A. Sumboja, J. Chen, Y. Ma, et al., ChemCatChem 11 (2019) 1205–1213.
[100] Y. Zhu, W. Zhou, Z. Shao, Small 13 (2017) 1603793.
[101] L.Y. Liang Y, H. Wang, Nat. Mater. 10 (2011) 780–786.
[102] W.H. Liang Y, J. Zhou, J. Am. Chem. Soc. 134 (2012) 3517–3523.
[103] M.G. Park, D.U. Lee, M.H. Seo, Small 12 (2016) 2707–2714.
[104] T. Ling, P. Da, X. Zheng, et al., Sci. Adv. 4 (2018) eaau6261.
[105] T. Huang, K. Jiang, D. Chen, G. Shen, Chin. Chem. Lett. 29 (2018) 553–563.
[106] H.B. Tao, L. Fang, J. Chen, et al., J. Am. Chem. Soc. 138 (2016) 9978–9985.
[107] C. Wei, Z. Feng, G.G. Scherer, et al., Adv. Mater. 29 (2017) 1606800.
[108] K. Huang, Y. Sun, Y. Zhang, et al., Adv. Mater. 31 (2019) e1801430.
[109] A. Chinnappan, D. Ji, C. Baskar, et al., J. Alloys Compd. 735 (2018) 2311–2317.
[110] D. Ji, J. Sun, L. Tian, et al., Adv. Funct. Mater. 30 (2020) 1910568.
[111] S. Peng, X. Han, L. Li, et al., Adv. Energy Mater. 8 (2018) 1800612.
[112] T. Zhou, W. Xu, N. Zhang, et al., Adv. Mater. 31 (2019) 1807468.
[113] Z. Jiang, Z.J. Jiang, T. Maiyalagan, A. Manthiram, J. Mater. Chem. A 4 (2016) 5877–5889.
[114] S. Zeng, X. Tong, S. Zhou, et al., Small 14 (2018) 1803409.
[115] X. Zheng, X. Han, H. Liu, et al., ACS Appl. Mater. Interfaces 10 (2018) 13675–13684.
[116] J. Suntivich, H.A. Gasteiger, N. Yabuuchi, et al., Nat. Chem. 3 (2011) 546–550.
[117] N. Xu, H. Zhao, X. Zhou, et al., Int. J. Hydrogen Energy 35 (2010) 7295–7301.
[118] J. Fu, D.U. Lee, F.M. Hassan, et al., Adv. Mater. 27 (2015) 5617–5622.
[119] T.V. Tam, S.G. Kang, M.H. Kim, et al., Adv. Energy Mater. (2019) 1900945.
[120] J. Zhang, M. Zhang, Y. Zeng, et al., Small 15 (2019) e1900307.
[121] J.I. Jung, M. Risch, S. Park, et al., Energy Environ. Sci. 9 (2016) 176.